Model for the orientational ordering of the plant microtubule cortical array

Rhoda J. Hawkins,[1,2,*] Simon H. Tindemans,[1,†] and Bela M. Mulder[1]
[1]*FOM Institute AMOLF, Science Park 104, 1098 XG Amsterdam, The Netherlands*
[2]*UMR 7600, Université Pierre et Marie Curie/CNRS, 4 Place Jussieu, 75255 Paris Cedex 05 France*
(Received 7 December 2009; published 19 July 2010)

The plant microtubule cortical array is a striking feature of all growing plant cells. It consists of a more or less homogeneously distributed array of highly aligned microtubules connected to the inner side of the plasma membrane and oriented transversely to the cell growth axis. Here, we formulate a continuum model to describe the origin of orientational order in such confined arrays of dynamical microtubules. The model is based on recent experimental observations that show that a growing cortical microtubule can interact through angle dependent collisions with pre-existing microtubules that can lead either to co-alignment of the growth, retraction through catastrophe induction or crossing over the encountered microtubule. We identify a single control parameter, which is fully determined by the nucleation rate and intrinsic dynamics of individual microtubules. We solve the model analytically in the stationary isotropic phase, discuss the limits of stability of this isotropic phase, and explicitly solve for the ordered stationary states in a simplified version of the model.

DOI: 10.1103/PhysRevE.82.011911 PACS number(s): 87.10.Ed, 87.16.ad, 87.16.Ka, 87.16.Ln

I. INTRODUCTION

Most plant cells grow by uniaxial expansion. Establishing and maintaining this characteristic anisotropic growth mode requires regulatory mechanisms that are robust, and, in addition, sensitive to the cell geometry. A major role in this process is played by microtubules, highly dynamic filamentous protein aggregates that form one of the components of the cytoskeleton of all eukaryotic organisms (see Ref. [1], chapter 16). In growing plant cells microtubules are confined to a thin layer of cytoplasm just inside the cell plasma membrane. Here, they form the so-called cortical array, an ordered structure formed by highly aligned (bundles of) microtubules oriented transversely to the growth direction [2]. This structure is unique to plant cells and there is evidence that it controls the direction of cell expansion by guiding the mobile transmembrane protein complexes that deposit long cellulose microfibrils in the plant cell wall [3]. These cellulose microfibrils are the main structural elements of the cell wall, which, for mechanical reasons, are also transversely oriented to the cell axis in growing cells [4]. An *in vivo* image of the array and a schematic are shown in Fig. 1. *In vivo* imaging of microtubules labeled with fluorescent proteins in plant cells by several groups has shown how the cortical array is established both following cell division and after microtubule depolymerizing drug (oryzalin) treatment [2,3,5–8]. In these studies microtubules are seen to nucleate at the cortex and then develop from an initially disorganized state into the transverse ordered array over a time period on the order of one hour. The nature of the self-organization process by which the specific spatial and orientational patterning of this cytoskeletal structure is achieved is as yet only partially understood and forms the subject of this work.

An important aspect of the problem is the nature of localization of the microtubules to the cortical region. Fluorescence recovery after photo-bleaching (FRAP) experiments by Shaw *et al.* [7] showed that the microtubules are fixed in space, so any apparent mobility of microtubules is due to "treadmilling," the process of simultaneous polymerization at one end and depolymerization at the other end. So, cortical microtubules do not translate or rotate as a whole. The same authors also did not detect detachment or (re)attachment of microtubules to the cell cortex, apart from some growing ends of single microtubules moving out of focus and found no evidence for motors working in the cortical array. These experiments indicate that the microtubules in the cortical array are fixed to the inside of the cell membrane. Electron microscopy has also shown cross-bridges between cortical microtubules and the membrane [9]. It is therefore widely assumed that there are linker proteins that anchor the microtubules through the plasma membrane to the rigid cell wall, although their molecular identity is under debate [10–14]. Since the cortical microtubules are effectively confined to a two-dimensional (2D) surface, they can interact through 'collisions' that occur when the polymerizing tip of a growing microtubule encounters a pre-existing microtubule. The resulting dynamical interaction events were first character-

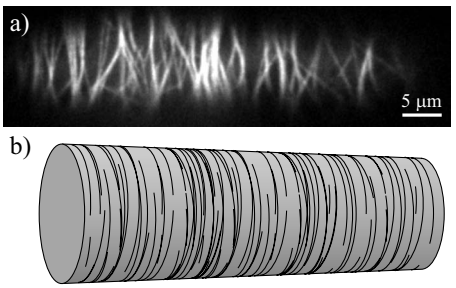

FIG. 1. (a) Fluorescently labeled microtubules in a Tobacco BY-2 cell expressing GFP:TUA6. Image courtesy of Jelmer Lindeboom, Wageningen University. (b) Schematic representation of a plant cell cortical array.

*Present address: Department of Mathematics, University of Bristol, Bristol, BS8 1TW, UK; rhoda.hawkins@physics.org
†Present address: Department of Electrical and Electronic Engineering, Imperial College London, South Kensington Campus, London SW7 2AZ, UK; s.tindemans@imperial.ac.uk

ized by Dixit and Cyr [15] in tobacco Bright Yellow-2 (BY-2) cells. They observed three different possible outcomes: (i) *zippering*: a growing microtubule bending toward the direction of the microtubule encountered, which occurs only when the angle of incidence is relatively small ($\lesssim 40°$) (ii) *induced catastrophe*: an initially growing microtubule switching to a shrinking state and retracting after the collision, an effect predominant at larger angles of incidence and (iii) *crossover*: a growing microtubule 'slipping over' the one encountered and continuing to grow in its original direction.

There are clearly many coupled mechanisms at work in this complex biological system, contributing to the assembly and maintenance of this microtubule cortical array structure. We are interested in understanding what are the main contributing factors and how their interplay leads to the observed orientational ordering. With this aim in mind we develop a coarse-grained model, incorporating all the effects discussed above. Our emphasis on the plant-specific biological mechanism of the ordering in the cortical array distinguishes our approach from earlier work.

Over the years, various models for self-organization of cytoskeletal filaments (and polar rods in general) have been proposed [16–21], and the model by Zumdieck *et al.* [22] was applied to the plant cortex. However, in each of these models the filaments are assumed to have rotational and, in most cases, translational degrees of freedom. This is inconsistent with the fact that the plant cortical microtubules are stably anchored. Inspired by the experimental results of Dixit and Cyr [15], Baulin *et al.* [23] report on a two-dimensional dynamical system of treadmilling and colliding microtubules. Their focus was on establishing the minimal interactions needed to generate dynamical alignment. Using simulations they showed that a pausing mechanism, whereby a growing microtubule stalls against another microtubule until the latter moves away, can indeed lead to ordering. Stalling, however, is not often observed in the cortical array. Moreover, their model lacks dynamic instabilities, i.e., catastrophes, both spontaneous and induced, and rescues, which is arguably unrealistic in view of the observed dynamics. Because of this, the microtubules will, in the absence of collisions, deterministically grow to infinite length, making it unlikely that stable aligned stationary phases actually exist in their system.

The outline of the paper is as follows. In Sec. II, we formulate our course-grained model starting from a description of the dynamics of individual microtubules. We then construct the continuity equations that couple the densities of growing, shrinking and inactive microtubule segments due to the intrinsic and collisional dynamics. In the steady state we can reduce the initial set of equations to four coupled nonlinear integral equations. We then perform a dimensional analysis to identify the relevant control parameter of the system. In Sec. III, we present the results of our model. We first solve the model analytically in the isotropic stationary state. Using a bifurcation analysis we then determine the critical values of the control parameter at which the system develops ordered solutions. We interpret these results in terms of the physical parameters of microtubule segment length and mesh size. Finally, we formulate a minimal model with realistic interaction parameters that we can solve numerically to obtain all stationary ordered solutions. We close by giving arguments for the stability of these solutions. The paper concludes with a discussion section. An appendix outlines further details of the numerical solution technique employed.

II. MODEL

A. Description of the microtubules and their dynamics

As described in the introduction we confine the configuration of the microtubules to a 2D plane. Since collision-induced zippering events can cause microtubules to bend along the direction of preexisting ones, we consider each microtubule to consist of a series of connected segments with a fixed orientation. We treat these segments as straight rigid rods. This is justifiable since the persistence length l_p of microtubules is long ($\sim$mm) compared to the average length of a microtubule ($\sim 10\ \mu$m) and, as mentioned above, adhesion to the plasma membrane further inhibits thermal motion.

Microtubules are known to be dynamic in that they are continually growing or shrinking by (de)polymerization. We use the standard two-state dynamic instability model of Dogterom and Leibler [24] which assumes that each microtubule has a "plus" end, located on the final segment of each microtubule, that is either growing (labeled by +) with speed v^+ or shrinking (labeled by −) with speed v^-. This plus end can switch stochastically from growing to shrinking (a so-called "catastrophe") with rate r_c, or from shrinking to growing (a so-called "rescue") with rate r_r in a process known as dynamic instability.

We model the creation of new microtubules with a constant, homogeneous, isotropic nucleation rate r_n in the plane of the 2D model. *In vivo* nucleation appears to occur at the cortex and has been observed to occur in random orientations unattached to pre-existing microtubules [7]. Although microtubules have also been observed to nucleate by γ-tubulin complexes binding to pre-existing microtubules [2,25,26] we ignore this possibility for simplicity's sake. By the same token we disregard the possibility of the shrinking of microtubules at their less active "minus" end, leading to motion through the "treadmilling" mechanism [27]. The initial segment of each microtubule therefore remains attached to the nucleation point in our model.

We call the final segment of a microtubule, which contains the growing or shrinking tip, *active* and all the remaining ones, which do not change their length, *inactive* (labeled by 0). A cartoon of an individual microtubule according to these definitions is depicted in Fig. 2 (see also the description of the parameters in Table I). When a microtubule collides with another microtubule and experiences a zippering event, its active segment is converted into an inactive segment, and a new active segment is created alongside the encountered microtubule. The inverse can also occur: if the active segment shrinks to zero length, a previously inactive segment in another direction can be reactivated. An induced catastrophe event simply causes the growing active segment to become a shrinking one, as is the case for spontaneous catastrophes. Finally, a crossover results in the growing active segment continuing to grow unperturbed.

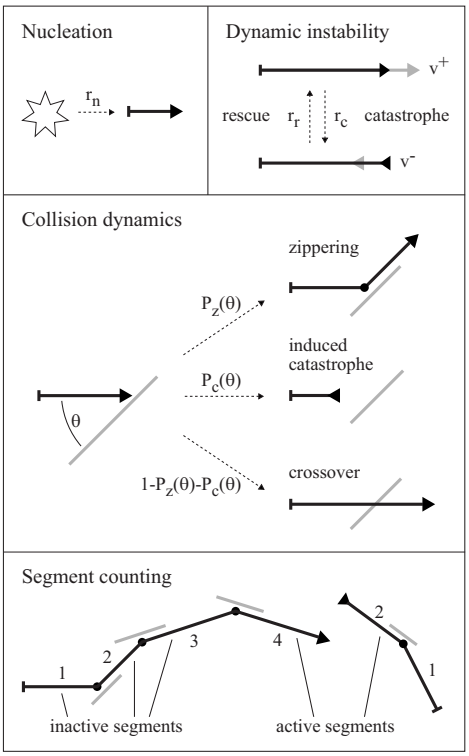

FIG. 2. Schematic representation of the model interaction. The microtubule of interest is drawn in black and other microtubules that it encounters are in gray. The active segments of the black microtubule have an arrow head indicating growth or shrinkage whereas inactive segments end in the junction with the following segment depicted by a dot.

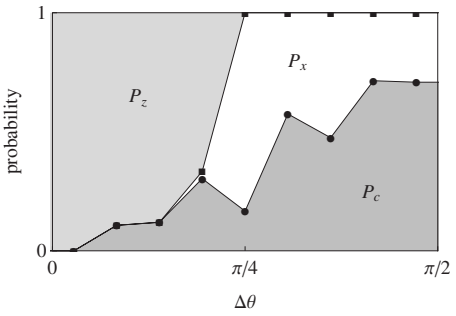

FIG. 3. Probabilities for zippering, crossovers and catastrophes as deduced from the observations of [15] (combined data from MBD-DsRed and YFP-TUA6 labeling). Light gray shaded region: fraction of zippering events. Dark gray shaded region: fraction of induced catastrophes. White region: fraction of crossovers. Every data point is located at the center of the corresponding bin, and the shaded regions have been extended to the boundaries using horizontal lines. The corresponding lowest order Fourier coefficients of the interaction functions are: $\hat{c}_0=0.59$, $\hat{c}_2=-0.36$, and $\hat{z}_0=0.24$ (computed using numerical integration of the product of $|\sin\theta|$ and a piecewise linear interpolation of the data).

In Fig. 3, we present the relative probabilities for zippering, induced catastrophes and crossovers as a result of collisions between microtubules, based on the data provided by Dixit and Cyr [15]. We assume that there are no microtubule polarity effects, as they were not reported. The probabilities $P_z(\theta-\theta')$, $P_x(\theta-\theta')$ and $P_c(\theta-\theta')$ for zippering, crossovers and induced catastrophes respectively are therefore even functions of the angle difference $\theta-\theta'$ defined by their values on the interval $[0,\frac{\pi}{2}]$. In this article we will use only the

TABLE I. Overview of all parameters and variables in natural dimensions. Experimental values for tobacco BY-2 cells in interphase from [36,10].

Parameters	Description	Dimensions	Experimental value
v^+	Growth speed	[length]/[time]	0.08 μm s^{-1}
v^-	Shrinkage speed	[length]/[time]	0.16–0.32 μm s^{-1}
r_c	Catastrophe rate	1/[time]	0.005–0.017 s^{-1}
r_r	Rescue rate	1/[time]	0.007–0.06 s^{-1}
r_n	Nucleation rate	[length]$^{-2}$[time]$^{-1}$	
$P_c(\theta)$	Probability of induced catastrophe upon collision	1	
$P_z(\theta)$	Probability of zippering upon collision	1	
Synthetic parameters			
$g=\frac{r_r}{v^-}-\frac{r_c}{v^+}$	Growth parameter	1/[time]	
$u=1+\frac{v^+}{v^-}$	Speed ratio	1	
$c(\theta)=\sin(\lvert\theta\rvert)P_c(\theta)\leftrightarrow\{\hat{c}_n\}$	Effective catastrophic collision probability	1	
$z(\theta)=\sin(\lvert\theta\rvert)P_z(\theta)\leftrightarrow\{\hat{z}_n\}$	Effective zippering probability	1	
Dependent variables			
$k(\theta)$	Microtubule length density	[length]$^{-1}$[radian]$^{-1}$	
$\bar{l}(\theta)$	Average microtubule Segment length	[length]	
$\{m_i^+(l,\theta),m_i^-(l,\theta),m_i^0(l,\theta)\}$	Density of growing/shrinking/inactive segmentswith length l and direction θ	[length]$^{-3}$[radian]$^{-1}$	

following minimal set of properties, which are qualitatively supported by the data. First, zippering becomes less likely for increasing angle of incidence, and is effectively zero at $\theta-\theta'=\frac{\pi}{2}$, which is reasonable as the energy associated with bending the microtubule increases with angle. Second, the probability for induced catastrophes monotonically increases with increasing angle of incidence, reaching a maximum at $\theta-\theta'=\frac{\pi}{2}$, consistent with observations that indicate that a microtubule which is hindered in its growth will undergo a catastrophe at a rate that depends inversely on its growth speed [28].

B. Continuum model

Since there are many ($\approx 10^2-10^3$) microtubules, each of which can have multiple segments, in the cortical array of a typical interphase plant cell we treat the system using a coarse-grained description. In this approach, instead of individual microtubules, we consider local densities of microtubule segments. This approximation is reasonable as long as the length scale of an individual microtubule segment is small compared to the linear dimensions of the cell. From the outset we assume that the system is (and remains) spatially homogeneous, and we will eventually restrict ourselves to the steady-state solutions. In our model, microtubules are made up of multiple connected segments, and the junctions between segments correspond to past zippering events where the microtubule has changed its growth direction. We introduce an index i to distinguish these segments of a microtubule, starting at 1 for the segment attached to the nucleation site and incremented for each subsequent segment. The recently nucleated $i=1$ segments are distributed isotropically, but segments with higher indices may acquire a preferred orientation as a result of the zippering interactions. Because the zippering dynamics of a growing tip are independent of the number, orientation and length of the segments behind it, the segments of a microtubule can be treated in isolation, with appropriate boundary conditions and connection properties. Our fundamental variables are therefore the areal number densities $m_i^\sigma(l,\theta,t)$ of segments in state $\sigma \in \{0,-,+\}$ with segment number i having length l and orientation θ (measured from an arbitrary axis) at time t. These densities obey a set of evolution equations that can symbolically be written as

$$\partial_t m_i^+(l,\theta,t) = \Phi_{growth} + \Phi_{rescue} - \Phi_{spont.\ cat.} - \Phi_{induced\ cat.} - \Phi_{zipper} \tag{1a}$$

$$\partial_t m_i^-(l,\theta,t) = \Phi_{shrinkage} - \Phi_{rescue} + \Phi_{spont.\ cat.} + \Phi_{induced\ cat.} + \Phi_{reactivation} \tag{1b}$$

$$\partial_t m_i^0(l,\theta,t) = +\Phi_{zipper} - \Phi_{reactivation}. \tag{1c}$$

The flux terms Φ_{event} couple the equations for the growing, shrinking and inactive segments and between different values of i. Equations (1a)–(1c) must be supplemented by a set of boundary conditions for the growing segments at $l=0$. For the initial segment ($i=1$) this reflects the isotropic nucleation of new microtubules, given by

$$v^+ m_1^+(l=0,\theta,t) = \frac{r_n}{2\pi}, \tag{2}$$

where r_n is nucleation rate. For subsequent segments $i>1$, the 'nucleation' of growing segments is the result of the zippering of segments with index $i-1$. Defining $\varphi_{zipper}^{i-1\to i}(\theta' \to \theta, l', t)$ as the flux of $(i-1)$-segments with angle θ' and length l' zippering into angle θ at time t [this is made explicit in Eq. (13)], we obtain the boundary condition

$$v^+ m_{i\geq 2}^+(l=0,\theta,t) = \int dl' \int d\theta' \varphi_{zipper}^{i-1\to i}(\theta' \to \theta, l', t). \tag{3}$$

In the general case, this leads to a different boundary condition on the density of growing segments for every value of i. The model therefore consists of an infinite set of coupled equations, three for every value of i. However, in Sec. II C, we will show that in the steady state we can explicitly sum our variables over the segment indices, reducing the infinite set to a finite set of 4 equations. In the following, we derive explicit expressions for each of the flux terms Φ_{event} in Eq. (1).

1. Growth and shrinkage terms: Φ_{growth} and $\Phi_{shrinkage}$

Φ_{growth} in Eq. (1a) corresponds to the length increase of the growing segments. For segment growth in isolation, the length increase in a small time interval δt is given by $v^+\delta t$, where v^+ is the growth velocity, and we have $m_i^+(l+v^+\delta t,\theta,t+\delta t)=m_i^+(l,\theta,t)$. By expanding the left hand term to first order in δt, we find

$$\partial_t m_i^+(l,\theta,t) = -v^+ \partial_l m_i^+(l,\theta,t) \equiv \Phi_{growth}. \tag{4}$$

A similar derivation yields that

$$\partial_t m_i^-(l,\theta,t) = v^- \partial_l m_i^-(l,\theta,t) \equiv \Phi_{shrink}, \tag{5}$$

where v^- is the shrinking velocity.

2. Dynamic instability terms: Φ_{rescue} and $\Phi_{spont.\ cat.}$

Φ_{rescue} and $\Phi_{spont.\ cat.}$ in Eqs. (1a) and (1b) correspond to the fluxes due to the spontaneous rescues and spontaneous catastrophe respectively and are simply given by

$$\Phi_{rescue} = r_r m_i^-(l,\theta,t) \tag{6}$$

$$\Phi_{spont.\ cat.} = r_c m_i^+(l,\theta,t), \tag{7}$$

where r_r is the spontaneous rescue rate and r_c is the spontaneous catastrophe rate.

So far, we have described the first three terms of Eqs. (1a) and (1b) (growth, shrinkage and dynamic instability terms). Together, these fully describe a system of non-interacting microtubules, in which also the boundary condition Eq. (3) vanishes due to the absence of zippering. In this special case, setting $m_i^\sigma=0$ for all $i\geq 2$, we recover the well-known equations introduced by Dogterom and Leibler [24].

3. Interaction terms: $\Phi_{induced\ cat.}$, Φ_{zipper}

An interaction can occur when a growing active microtubule segment collides with another segment, irrespective of

the latter's state and length. This prompts the definition of the total length density $k(\theta,t)$ of all microtubule segments in direction θ at time t, given by

$$k(\theta,t) = \sum_i \int \mathrm{d}l\, l[m_i^+(l,\theta,t) + m_i^-(l,\theta,t) + m_i^0(l,\theta,t)]. \quad (8)$$

The density of collisions of a microtubule segment growing in direction θ with other segments in direction θ' is determined by the perpendicular projection of the length density onto the path of the incoming segment:

$$|\sin(\theta-\theta')|k(\theta',t). \quad (9)$$

When a collision occurs, one of the three possible events, induced catastrophe (c), zippering (z) or crossover (x) occurs, with probabilities $P_c(\theta-\theta')$, $P_z(\theta-\theta')$, and $P_x(\theta-\theta')$, respectively. These probabilities can (and *in-vivo* do, see Fig. 3) depend on the relative angle $\theta-\theta'$ between the incoming segment and the "scatterer." For convenience sake we absorb the geometrical factor $|\sin(\theta-\theta')|$ into the probabilities, by defining $f(\theta-\theta')=|\sin(\theta-\theta')|P_f(\theta-\theta')$ for all events $f \in \{c,z,x\}$. The incoming flux of growing microtubule segments with given segment number, length and orientation is given by $v^+m_i^+(l,\theta,t)$. With these definitions we can write the interaction terms as

$$\Phi_{\text{induced cat.}} = v^+m_i^+(l,\theta,t)\int d\theta' c(\theta-\theta')k(\theta',t) \quad (10)$$

$$\Phi_{\text{zipper}} = v^+m_i^+(l,\theta,t)\int d\theta' z(\theta-\theta')k(\theta',t). \quad (11)$$

The analogous term for crossovers is not used, because the occurrence of a crossover event has no effect on the growth of a microtubule.

4. Reactivation term: $\Phi_{reactivation}$

Shrinking microtubules will necessarily shrink back along the paths they grew along. This includes undoing any zippering events that may have occurred in the past. In this sense the microtubules retain a nontrivial memory of their paths, which should be addressed by the model. Here, we derive an implicit expression for this "unzippering" process. In the following paragraph we will then show how a balance law that follows from the steady state assumption allows us to obtain an explicit expression for the contribution of this process in terms of the model variables.

When active segments with index $i+1$ shrink to zero length, they reactivate inactive segments with index i, effectively undoing the zippering event that created the $i+1$ segment in the past. The $i+1$ segment is removed and an inactive i segment is converted into a shrinking i segment. The reactivation term $\Phi_{\text{reactivation}}$ describes the conversion flux from inactive to active segments with segment index i. We note that the (forward) zippering process is independent of the properties (length and angle) of the previous segments. This implies that the correlations between segment orientations can be fully expressed in terms of pairs of subsequent indices, i.e., i and $i+1$. As a result, the reactivation flux (reverse zippering process) can be computed using only quantities related to the segment indices i and $i+1$.

The incoming flux of shrinking segments coming from a given direction θ' is given by $v^-m_{i+1}^-(l'=0,\theta',t)$. The reactivation flux is given by

$$\Phi_{\text{reactivation}} = \int d\theta' v^- m_{i+1}^-(l'=0,\theta',t)p_{\text{unzip}}^{i+1\to i}(\theta,l|\theta',t), \quad (12)$$

where the unzippering distribution $p_{\text{unzip}}^{i+1\to i}(\theta,l|\theta',t)$ gives the probability that the shrinking microtubule reactivates an inactive segment with orientation θ and length l. This distribution will be determined below.

A microtubule that has zippered will take a certain amount of time τ to undergo a catastrophe and return to the zippering location, where τ is a stochastic variable. The unzipppering flux from direction θ' at time t consists of microtubules that had zippered at a range of times $t-\tau$ and have now returned to the zippering location. This implicitly defines an *originating time* distribution $p_{\text{origin}}^{i+1}(t-\tau|\theta',t)$ for the returning microtubules. Furthermore, because the evolution of a microtubule between the zippering event and its return to the same location does not depend on the previous segments, the segment that is reactivated by a microtubule returning to the zippering position after a time τ should be selected proportional to the "forward" zippering flux at time $t-\tau$. The forward flux $\varphi_{\text{zipper}}^{i\to i+1}(\theta\to\theta',l,t)$ of microtubules with length l and angle θ zippering into angle θ' is defined in accordance with Eq. (11) as

$$\varphi_{\text{zipper}}^{i\to i+1}(\theta\to\theta',l,t) = v^+m_i^+(l,\theta,t)z(\theta-\theta')k(\theta',t). \quad (13)$$

At each of the originating times $t-\tau$, the distribution of microtubules that zipper into the direction θ' with length l and orientation θ is given by

$$p_{\text{zip}}^{i\to i+1}(\theta,l|\theta',t-\tau) = \frac{\varphi_{\text{zipper}}^{i\to i+1}(\theta\to\theta',l,t-\tau)}{\int dl''d\theta''\varphi_{\text{zipper}}^{i\to i+1}(\theta''\to\theta',l'',t-\tau)}. \quad (14)$$

The probability distributions $p_{\text{origin}}^{i+1}(t-\tau|\theta',t)$ and $p_{\text{zip}}^{i\to i+1}(\theta,l|\theta',t-\tau)$ can be combined to determine the unzippering distribution

$$p_{\text{unzip}}^{i+1\to i}(\theta,l|\theta',t) = \int_0^t d\tau p_{\text{origin}}^{i+1}(t-\tau|\theta',t)p_{\text{zip}}^{i\to i+1}(\theta,l|\theta',t-\tau), \quad (15)$$

where we assume the system evolved from an initial condition at $t_0=0$ in which no microtubules were present. Clearly all the complicated history dependence of the system is hidden in the originating time distribution. However, in the steady state situation we consider below, the time-dependence drops out and the details of this distribution become irrelevant.

C. Steady state

We now consider the steady state of the system of equations we have formulated. Setting the time derivatives to zero, the sum of Eqs. (1a)–(1c) yields $\Phi_{growth}+\Phi_{shrinkage}=0$, which together with Eqs. (4) and (5) implies $\partial_l[v^+m_i^+(l,\theta)-v^-m_i^-(l,\theta)]=0$. Because physically acceptable solutions should be bounded as $l\to\infty$, we obtain the length flux balance equation

$$v^+m_i^+(l,\theta)=v^-m_i^-(l,\theta), \tag{16}$$

showing that the growing and shrinking segments have, up to a constant amplitude, the same orientational and length distribution. This allows us to eliminate $m_i^-(l,\theta)$ from Eq. (1a) to obtain

$$\partial_l m_i^+(l,\theta)=m_i^+(l,\theta)\times\left\{g-\int d\theta'[c(|\theta-\theta'|)+z(|\theta-\theta'|)]k(\theta')\right\}, \tag{17}$$

where the *growth parameter*

$$g=\frac{r_r}{v^-}-\frac{r_c}{v^+}, \tag{18}$$

characterizes the behavior of the bare, noninteracting, system in which microtubules remain bounded in length for $g<0$ and become unbounded for $g\geq 0$. As the bracketed factor on the right hand side of Eq. (17) does not depend on the segment length nor on the segment number, we immediately obtain that $m_i^+(l,\theta)$ has an exponential length distribution

$$m_i^+(l,\theta)=m_i^+(\theta)e^{-l/\bar{l}(\theta)}, \tag{19}$$

where the average segment length $\bar{l}(\theta)$ in the direction θ is given by

$$\frac{1}{\bar{l}(\theta)}=-g+\int d\theta'[c(\theta-\theta')+z(\theta-\theta')]k(\theta'). \tag{20}$$

The nucleation boundary conditions Eqs. (2) and (3) are now transformed into independent nucleation equations that are expressed in terms of the amplitudes $m_i^+(\theta)$

$$v^+m_1^+(\theta)=\frac{r_n}{2\pi}, \tag{21}$$

$$m_{i\geq 2}^+(\theta)=k(\theta)\int d\theta' z(\theta'-\theta)\bar{l}(\theta')m_{i-1}^+(\theta'). \tag{22}$$

We show here that in the steady state the flux-balance equation for the inactive segments Eq. (1c) is automatically satisfied. Inserting Eqs. (14) and (15) into the definition of the reactivation flux $\Phi_{reactivation}$ [Eq. (12)] becomes;

$$\Phi_{reactivation}=\int d\theta'\left\{v^-m_{i+1}^-(l'=0,\theta',t)\times\int_0^t d\tau\left\{p_{origin}^{i+1}(t-\tau|\theta',t)\times\frac{\varphi_{zipper}^{i\to i+1}(\theta\to\theta',l,t-\tau)}{\int dl''d\theta''\varphi_{zipper}^{i\to i+1}(\theta''\to\theta',l'',t-\tau)}\right\}\right\}.$$

In the steady state $\varphi_{zipper}^{i\to i+1}$ and $m_{i+1}^-(l',\theta',t)$ are independent of time. Using this fact and the flux balance Eq. (16) gives

$$\Phi_{reactivation}=\int d\theta'\left\{v^+m_{i+1}^+(l'=0,\theta')\times\frac{\varphi_{zipper}^{i\to i+1}(\theta\to\theta',l)}{\int dl''d\theta''\varphi_{zipper}^{i\to i+1}(\theta''\to\theta',l'')}\times\int_0^t d\tau p_{origin}^{i+1}(t-\tau|\theta',t)\right\}.$$

The system approaches the steady state as $t\to\infty$, and the integral over all time of p_{origin} is by definition unity, leading to

$$\Phi_{reactivation}=\int d\theta'\left\{v^+m_{i+1}^+(l'=0,\theta')\times\frac{v^+m_i^+(l,\theta)z(\theta-\theta')k(\theta')}{\int dl''d\theta''v^+m_i^+(l'',\theta')z(\theta''-\theta')k(\theta')}\right\},$$

where $\varphi_{zipper}^{i\to i+1}$ has been replaced by its definition from Eq. (13). Finally we use Eq. (19) and (22) to give

$$\Phi_{reactivation}=\int d\theta'\left\{v^+k(\theta')\int d\theta z(\theta-\theta')\bar{l}(\theta)m_i^+(\theta)\times\frac{v^+m_i^+(l,\theta)z(\theta-\theta')k(\theta')}{\int d\theta v^+\bar{l}(\theta)m_i^+(\theta)z(\theta-\theta')k(\theta')}\right\}.$$

$$=\int d\theta' v^+m_i^+(l,\theta)z(\theta-\theta')k(\theta')=\Phi_{zipper}$$

and therefore reproducing Eq. (1c) for the steady state.

Since Eq. (1c) is automatically satisfied we need an independent argument to fix the densities of the inactive segments. To obtain this we use the steady state rule that population size=nucleation rate×average lifetime. Con-

sider a newly 'born' growing segment, created either by a nucleation or a zippering event. Its average life time is by definition the average time until it shrinks back to zero length, i.e., the average return time. Clearly this time only depends on its orientation θ, the steady state microtubule length density $k(\theta')$ and the dynamical instability parameters, but not on the segment number. We therefore denote the average segment lifetime by $\tau(\theta)$. The steady state density of inactive segments with length l, orientation θ and segment number i is then given by

$$m_i^0(l,\theta) = \int d\theta' \varphi_{\text{zipper}}^{i\to i+1}(\theta \to \theta', l)\tau(\theta'), \tag{23}$$

where $\varphi_{\text{zipper}}^{i\to i+1}$ is defined by Eq. (13), as inactive segments are created by a zippering event. Because the only length-dependent term on the right-hand side is $m_i^+(l,\theta)$, it follows that the length dependence of the inactive segment distributions is proportional to those of the active segments, i.e.,

$$m_i^0(l,\theta) = m_i^0(\theta)e^{-l/\bar{l}(\theta)}. \tag{24}$$

At the same time, the total integrated length density of segments, both active and inactive, with segment number $i+1$ in the direction θ' is given by

$$N_{i+1}^{\text{total}}(\theta') = \int dl'[m_{i+1}^0(l',\theta') + m_{i+1}^+(l',\theta') + m_{i+1}^-(l',\theta')] \tag{25a}$$

$$= \int d\theta \int dl \varphi_{\text{zipper}}^{i\to i+1}(\theta \to \theta', l)\tau(\theta'), \tag{25b}$$

where the equality Eq. (25b) follows from the fact that every segment with index $i+1$ has been created by a zippering event of a segment with index i. We solve Eq. (25a) for $\tau(\theta')$ and insert the result in Eq. (23), which, after expanding $\varphi_{\text{zipper}}^{i\to i+1}$ [Eq. (13)] and N_{i+1}^{total} [Eq. (25a)] and integrating both sides over l, produces the following expression for $m_i^0(\theta)$:

$$m_i^0(\theta) = m_i^+(\theta)\int d\theta' z(\theta-\theta')\bar{l}(\theta') \times \frac{[m_{i+1}^0(\theta') + m_{i+1}^+(\theta') + m_{i+1}^-(\theta')]}{\int d\theta z(\theta-\theta')\bar{l}(\theta)m_i^+(\theta)}.$$

The nucleation Eq. (22) can be used to replace the integral in the denominator of the integrand on the right hand side of this expression:

$$m_i^0(\theta) = m_i^+(\theta)\int d\theta' z(\theta-\theta')\bar{l}(\theta') \times \frac{[m_{i+1}^0(\theta') + m_{i+1}^+(\theta') + m_{i+1}^-(\theta')]}{m_{i+1}^+(\theta')/k(\theta')}. \tag{26}$$

We now define the quantity $Q_i(\theta)$ through

$$m_i^0(\theta) = Q_i(\theta)[m_i^+(\theta) + m_i^-(\theta)] = \left(1+\frac{v^+}{v^-}\right)Q_i(\theta)m_i^+(\theta) \equiv uQ_i(\theta)m_i^+(\theta), \tag{27}$$

where we implicitly defined $u=(1+\frac{v^+}{v^-})$. Substituting Eq. (26) into this definition of $Q_i(\theta)$ (27) gives

$$Q_i(\theta) = \frac{m_i^0(\theta)}{um_i^+(\theta)} = \int d\theta' \left\{ z(\theta-\theta')\bar{l}(\theta')k(\theta') \times \frac{[m_{i+1}^0(\theta') + m_{i+1}^+(\theta') + m_{i+1}^-(\theta')]}{um_{i+1}^+(\theta')} \right\}.$$

Rewriting $m_{i+1}^0(\theta')$ and $m_{i+1}^-(\theta')$ in terms of $m_{i+1}^+(\theta')$ using Eqs. (27) and (16) leads to the following recursion relation for $Q_i(\theta)$

$$Q_i(\theta) = \int d\theta' z(\theta-\theta')k(\theta')\bar{l}(\theta')[1+Q_{i+1}(\theta')]. \tag{28}$$

We now argue that the ratio $Q_i(\theta)$ is in fact independent of the segment number. Using the fact that the growing, shrinking and inactive segments have an identical exponential profile, it follows from Eq. (27) that $Q_i(\theta)$ is equal to the ratio between inactive and active segments

$$Q_i(\theta) = \frac{m_i^0(\theta)}{um_i^+(\theta)} = \frac{N_i^0(\theta)}{N_i^+(\theta)+N_i^-(\theta)}. \tag{29}$$

After a new microtubule segment has been created it will generally spend some time in an active state and some time in an inactive state. The expected lifetime $\tau(\theta)$ can also be separated into the expected active and inactive lifetimes for any newly created segment: $\tau(\theta)=\tau_{\text{active}}(\theta)+\tau_{\text{inactive}}(\theta)$. These lifetimes are necessarily proportional to the total number of active and inactive segments, so that $Q_i(\theta) = \tau_{\text{inactive}}(\theta)/\tau_{\text{active}}(\theta)$. As we have argued before, these lifetimes do not depend on the segment number, and, hence, neither does $Q_i(\theta)$. An alternative route to the same conclusion follows from expanding out the forward recursion in Eq. (28) to show that $Q_i(\theta)$ can for every i formally be written as the same infinite series of multiple integrals involving $z(\theta-\theta')$, $k(\theta)$ and $\bar{l}(\theta)$. We therefore write the self-consistency relationship

$$Q(\theta) = \int d\theta' z(\theta-\theta')k(\theta')\bar{l}(\theta')(1+Q(\theta')). \tag{30}$$

The final closure of this set of equations is provided by the definition of the length density Eq. (8) applied to the steady state

$$k(\theta) = \sum_i \int dl\, l[m_i^+(l,\theta) + m_i^-(l,\theta) + m_i^0(l,\theta)] = u\bar{l}(\theta)^2[1+Q(\theta)]\sum_i m_i^+(\theta). \tag{31}$$

It is useful to define the overall density of active segments (or, equivalently, the density of MT plus ends)

$$t(\theta) = \sum_{i=1}^{\infty} \int_0^{\infty} dl[m_i^+(l,\theta) + m_i^-(l,\theta)] = u\bar{l}(\theta) \sum_{i=1}^{\infty} m_i^+(\theta). \tag{32}$$

Using this definition and by taking the sum over the set of nucleation Eqs. (22), we obtain a closed form equation for the plus-end density

$$t(\theta) = u\bar{l}(\theta) m_1^+(\theta) + \bar{l}(\theta) k(\theta) \int d\theta' z(\theta' - \theta) t(\theta'), \tag{33}$$

where $m_1^+(\theta)$ is fixed by the imposed nucleation rate Eq. (21).

D. Dimensional analysis

In order to simplify our equations for further analysis and to identify the relevant control parameter we perform a dimensional analysis. We therefore introduce a common length scale and rescale all lengths with respect to this length scale. For example, our primary variables $m_i^+(\theta)$ have dimension $[\text{length}]^{-3}[\text{radian}]^{-1}$. Taking our cue from Eqs. (21) and (31) we adopt the length scale

$$l_0 = \left(\frac{1}{\pi} \frac{v^+}{u r_n/(2\pi)} \right)^{1/3}, \tag{34}$$

where the additional factor of π^{-1} within the parentheses is added to suppress explicit factors involving π in the final equations. This definition allows us to define the dimensionless variables

$$L(\theta) = \bar{l}(\theta)/l_0 \tag{35a}$$

$$K(\theta) = \pi k(\theta) l_0 \tag{35b}$$

$$T(\theta) = \pi l_0^2 t(\theta) \tag{35c}$$

$$G = g l_0. \tag{35d}$$

In the absence of interactions, Eq. (20) shows that when $g < 0$ the average length $\bar{l}$ of a microtubule is given by $\bar{l} = -1/g$. In that case we have $G = -l_0/\bar{l}$, meaning that, for $G < 0$, G can be interpreted as a measure for the noninteracting microtubule length.

In addition, we adopt the dimensionless operator notation

$$\mathbf{F}[h](\theta) = \frac{1}{\pi} \int_0^{2\pi} d\theta' f(\theta - \theta') h(\theta'), \tag{35e}$$

where $F \in \{C, Z\}$.

Applying the above definitions to the segment length Eq. (20), the density Eq. (31), the inactive/active ratio Eq. (30) and the plus-end density Eq. (33) respectively, our final set of dimensionless equations reads

Segment length:

$$\frac{1}{L(\theta)} = -G + \mathbf{C}[K](\theta) + \mathbf{Z}[K](\theta) \tag{36a}$$

Density:

$$K(\theta) = L(\theta)[1 + Q(\theta)] T(\theta) \tag{36b}$$

Inactive-active ratio:

$$Q(\theta) = \mathbf{Z}[LK(1+Q)](\theta) \tag{36c}$$

Plus end density:

$$T(\theta) = L(\theta) + L(\theta) K(\theta) \mathbf{Z}[T](\theta) \tag{36d}$$

with

$$G = \left[\frac{2v^+v^-}{r_n(v^+ + v^-)} \right]^{1/3} \left(\frac{r_r}{v^-} - \frac{r_c}{v^+} \right). \tag{36e}$$

Looking at the resulting equations, we see that the segment length L is determined by the intrinsic growth dynamics (G) and the collisions leading to induced catastrophes and zippering. The segment length density K is the product of the plus end density, the ratio of all segments to active segments $(1+Q)$ and the average segment length. The ratio Q of inactive to active segments is modulated by the zippering operator, and the plus end density T consists of contributions from direct nucleation and zippered segments. Obviously, we must restrict ourselves to parameter regions admitting physically realizable solutions, which have real and positive values for L, K, Q, and T.

Finally, we note that the interaction operators defined by Eq. (35e) are convolutions of the operand with the interaction functions $c(\theta)$ and $z(\theta)$. Both interaction functions are symmetric and π periodic, and can therefore be written in terms of their Fourier coefficients as

$$f(\theta) = \frac{\hat{f}_0}{2} + \sum_{n=1}^{\infty} \hat{f}_{2n} \cos(2n\theta), \tag{37}$$

$$\hat{f}_{2n} = \frac{1}{\pi} \int_0^{2\pi} d\theta f(\theta) \cos(2n\theta). \tag{38}$$

Using the identity $\cos(\theta - \theta') = \cos(\theta)\cos(\theta') + \sin(\theta)\sin(\theta')$ we find that the functions $\cos(2n\theta)$ and $\sin(2n\theta)$ are eigenfunctions of the operators $\mathbf{C}$ and $\mathbf{Z}$, with the Fourier coefficients $\hat{c}_{2n}$ and $\hat{z}_{2n}$, respectively, as eigenvalues:

$$\mathbf{F}[\cos(2n\theta)] = \hat{f}_{2n} \cos(2n\theta). \tag{39}$$

This convenient property will be exploited in later sections.

III. RESULTS

A. Isotropic solution

In the isotropic phase all angular dependence drops out. Because $\mathbf{C}[1] = \hat{c}_0$ and $\mathbf{Z}[1] = \hat{z}_0$ we are left with the set of equations

$$\frac{1}{\bar{L}} = -G + (\hat{c}_0 + \hat{z}_0)\bar{K} \tag{40a}$$

$$\bar{K} = \bar{L}(1+\bar{Q})\bar{T} \tag{40b}$$

$$\bar{Q} = \hat{z}_0 \bar{L}\bar{K}(1+\bar{Q}) \tag{40c}$$

$$\bar{T} = \bar{L} + \hat{z}_0 \bar{L}\bar{K}\bar{T}, \tag{40d}$$

where the overbar denotes quantities evaluated in the isotropic phase. Solving for $\bar{Q}$ and $\bar{T}$ and inserting this into Eq. (40b) readily gives

$$\bar{K} = \frac{\bar{L}^2}{(1-\hat{z}_0\bar{L}\bar{K})^2}, \tag{41}$$

which can be combined with Eq. (40a) to yield the following relationship between G and the density

$$\bar{K}(\hat{c}_0\bar{K} - G)^2 = 1. \tag{42}$$

We see that the isotropic density is an increasing function of the microtubule dynamics parameter G and does not depend on the amount of zippering. This can be understood by the fact that zippering only serves to reorient the microtubules, which has no net effect in the isotropic state. In the presence of induced catastrophes a stationary isotropic solution exists for all values of G, although this solution need not actually be stable.

In the absence of induced catastophes ($\hat{c}_0=0$), the microtubule lengths are bounded only by the spontaneous catastrophes. In this case, as $G\to 0$ the spontaneous catastrophes are increasingly counterbalanced by the rescue events, resulting in a divergence of the average microtubule length, as already shown by Dogterom and Leibler [24]. Assuming a constant nucleation rate, the corresponding increase in microtubule lifetime also leads to a diverging number of microtubules in the system. The diverging number and length of microtubules implies that the density K diverges, which is reflected in Eq. (42). In the biological cell such an unbounded increase in density would not be sustained since the necessarily finite pool of tubulin dimers will eventually be depleted, leading to a decrease in growth speeds and nucleation rates. In our model we assume constant growth and shrinkage rates thus implicitly assuming an infinite pool of tubulin dimers.

B. Bifurcation analysis

We now search for a bifurcation point by considering the existence of steady-state solutions, which are small perturbations away from the isotropic solution. These solutions are parametrized as follows

$$L = \bar{L}(1+\lambda) \tag{43a}$$

$$K = \bar{K}(1+\kappa) \tag{43b}$$

$$Q = \bar{Q}(1+\chi) \tag{43c}$$

$$T = \bar{T}(1+\tau). \tag{43d}$$

Inserting these expressions into Eq. (35e), subtracting the isotropic solutions and expanding to first order in the perturbations gives

$$\lambda = -\bar{N}(\mathbf{C}[\kappa] + \mathbf{Z}[\kappa]) \tag{44a}$$

$$\kappa = \lambda + \tau + \hat{z}_0\bar{N}\chi \tag{44b}$$

$$\chi = \frac{1}{\hat{z}_0}\mathbf{Z}[\lambda + \kappa + \hat{z}_0\bar{N}\chi] \tag{44c}$$

$$\tau = \lambda + \bar{N}(\hat{z}_0\kappa + \mathbf{Z}[\tau]), \tag{44d}$$

where $\bar{N}=\bar{L}\bar{K}$. Note that in these equations, $\bar{N}$ has become the control parameter instead of G. Using Eq. (44b) and exploiting the linearity of $\mathbf{Z}$, we expand

$$\mathbf{Z}[\kappa] = \mathbf{Z}[\tau] + \mathbf{Z}[\lambda + \kappa + \hat{z}_0\bar{N}\chi] - \mathbf{Z}[\kappa] \tag{45}$$

$$= \frac{1}{\bar{N}}(\tau - \lambda) - \hat{z}_0\kappa + \hat{z}_0\chi - \mathbf{Z}[\kappa]. \tag{46}$$

Solving this for $\mathbf{Z}[\kappa]$ and inserting the result into Eq. (44a), combined with Eq. (44b), yields the relation

$$(1-\hat{z}_0\bar{N})\kappa = -2\bar{N}\mathbf{C}[\kappa] \tag{47}$$

In the *absence* of induced catastrophes ($\mathbf{C}[\kappa]=0$; only zippering), a bifurcation could only occur if $\hat{z}_0\bar{N}=1$, which, from Eqs. (41) and (42), implies that the length density diverges (at $G=0$), thus, ruling out a physically acceptable bifurcation. This result shows that zippering by itself is unable to drive a transition to an ordered state.

In the generic case where induced catastrophes are present, Eq. (47) can be satisfied only if $\kappa(\theta)$ is an eigenfunction of $\mathbf{C}$. We know that the family of functions $\cos(2n\theta)$, $n\geq 1$, are eigenfunctions of $\mathbf{C}$ with eigenvalues $\hat{c}_{2n}$, and therefore get a set of bifurcation values for $\bar{N}$, one for each eigenvalue: $N^*_{2n}=(-2\hat{c}_{2n}+\hat{z}_0)^{-1}$. In addition, we know that the isotropic solution must be stable as $G\to-\infty$, because in this limit the microtubules have a vanishing length and do not interact. Therefore, the relevant bifurcation point is that for the lowest value of G, corresponding with the most negative eigenvalue of $\mathbf{C}$ (see also Sec. III E). Assuming that the induced catastrophe probability increases monotonically with the collision angle, $\hat{c}_2$ is always the most negative eigenvalue, so

$$N^* = \frac{1}{-2\hat{c}_2 + \hat{z}_0}. \tag{48}$$

We now derive the location of this bifurcation point in terms of the control parameter G. Denoting $\bar{N}=\bar{L}\bar{K}$, Eq. (41) can be transformed to $\bar{N}(1-\hat{z}_0\bar{N})^2=\bar{L}^3$, into which we can substitute $G\bar{L}=(\hat{c}_0+\hat{z}_0)\bar{N}-1$ from Eq. (40a) and solve for G giving

$$G^3\bar{N}(1-\hat{z}_0\bar{N})^2=[(\hat{c}_0+\hat{z}_0)\bar{N}-1]^3 \tag{49}$$

Combining this with the result Eq. (48) yields

$$G^*=(-2\hat{c}_2)^{1/3}\left(\frac{\hat{c}_0}{-2\hat{c}_2}-1\right). \tag{50}$$

The implication is that the location of the bifurcation point as a function of the control parameter G is determined entirely by the eigenvalues of the induced catastrophe function $c(\theta)$. Like the density in the isotropic phase, the location of the bifurcation point, this time perhaps more surprisingly, does not depend on the presence or amount of zippering.

C. Segment length and mesh size

An attractive interpretation of the microtubule length density $K(\theta)$ is that it represents the density of "obstacles" that are pointing in the direction θ as seen by a microtubule growing in the perpendicular direction. From the obstacle density we can define a mesh size $\xi(\theta)$—the average distance between obstacles. Taking into account the geometrical factor $\sin(\theta)$, we obtain

$$\xi(\theta)=\left[\frac{1}{\pi l_0}\int_0^{2\pi}d\theta'|\sin(\theta-\theta')|K(\theta')\right]^{-1}. \tag{51}$$

In the case of the isotropic solution, this simplifies to $\bar{\xi}=\pi l_0/(4\bar{K})$. Using this equality we can derive an expression for the average microtubule length $\bar{\Lambda}$ in the isotropic phase, expressed in units of the mesh size. The length of each segment is given by $\bar{L}$ and the number of segments per microtubule is given by $(1+\bar{Q})$, so using Eq. (41) we find

$$\bar{\Lambda}=\frac{l_0\bar{L}(1+\bar{Q})}{\bar{\xi}}=\frac{4\bar{K}^{3/2}}{\pi} \tag{52}$$

Inserting this result into Eq. (42) provides the relationship between $\bar{\Lambda}$ and G

$$G=\left(\frac{4}{\pi\bar{\Lambda}}\right)^{1/3}\left(\frac{\pi\hat{c}_0\bar{\Lambda}}{4}-1\right). \tag{53}$$

As was the case for the density, we see that the microtubule length as a function of mesh size does not depend on the amount of zippering. However, it should be noted that the mesh size is defined through the average distance between single microtubules. In real systems, zippering would naturally lead to bundling, which in turn produces a system that has a larger mesh size between bundles (see also the discussion).

Combining Eqs. (52) and (48), the expression for $\bar{\Lambda}$ at the bifurcation point becomes

$$\bar{\Lambda}^*=-\frac{2}{\pi\hat{c}_2} \tag{54}$$

Assuming a monotonically increasing induced catastrophe probability $P_c(\theta)$, we know that the minimum value for $\hat{c}_2$ is reached when every collision at an angle larger than 45° leads to a catastrophe. From Eq. (54), we see that this implies $\Lambda^*\geq 3/(2\sqrt{2})$, meaning that for a bifurcation to occur, the microtubules need to be longer (sometimes much longer) than the mesh size, as is to be expected.

Equation (53) can also provide an interpretation of the length scale l_0 in the case $g<0$. In the absence of catastrophic collisions, we find in this case

$$\bar{\Lambda}|_{\hat{c}_0=0}=\frac{4}{\pi}(-G^{-3})=\frac{4}{\pi}\left(\frac{\bar{l}}{l_0}\right)^3, \tag{55}$$

where $\bar{l}=-1/g$ is the average length of the microtubules. l_0 is therefore a measure of the microtubule length that is required to enable a significant number of interactions ($\bar{\Lambda}=4/\pi$ for $\bar{l}=l_0$). If the free microtubule average length $\bar{l}$ is (much) shorter than l_0, the system is dominated by the (isotropic) nucleations, keeping the system in an isotropic state. On the other hand, when $\bar{l}\gg l_0$, the interactions dominate and, depending on the interaction functions, the system has the potential to align.

D. Ordered solutions for simplified interaction functions

To find solutions beyond the immediate vicinity of the bifurcation point, we are hampered by the fact that these solutions are part of an infinite-dimensional solution space. In Appendix it is shown that the solutions can be constrained to a finite-dimensional space by restricting the interaction functions $c(\theta)$ and $z(\theta)$ to a finite number of Fourier modes.

In this section, we define a set of simplified interaction functions by restricting ourselves to Fourier modes up to and including $\cos(4\theta)$. These modes provide us with just enough freedom for the model to exhibit rich behavior. Using the fact that $c(0)=z(0)=z(\pi/2)=0$, we find that $\hat{z}_2=0$ and that both $\hat{z}_4$ and $\hat{c}_4$ are determined by the remaining parameters. Furthermore, we introduce an overall factor of α in both equations, allowing us to set $c(\pi/2)=\alpha$, so that $\hat{c}_2=-\alpha/2$. We thus obtain a system that is fully specified by the parameters $\hat{c}_0$, $\hat{z}_0$ and α.

$$c(\theta)=\alpha\left[\frac{\hat{c}_0}{2}-\frac{1}{2}\cos(2\theta)+\frac{1}{2}(1-\hat{c}_0)\cos(4\theta)\right] \tag{56a}$$

$$z(\theta)=\alpha\left\{\frac{\hat{z}_0}{2}[1-\cos(4\theta)]\right\}. \tag{56b}$$

For $\alpha=1$, $\hat{c}_0$ and $\hat{z}_0$ are the actual Fourier coefficients of the interaction functions. Demanding that $P_c(\theta)=c(\theta)/\sin(\theta)$ is monotonically increasing on the interval $[0,\pi/2]$ leads to the constraint

$$\frac{3}{4}\leq\hat{c}_0\leq\frac{9}{8} \tag{57}$$

and $\hat{z}_0$ is a positive real number. Of course, the total probability of zippering and catastrophe induction may not exceed 1, placing an upper bound on α. In the absence of zippering, we have $\alpha\leq 1$.

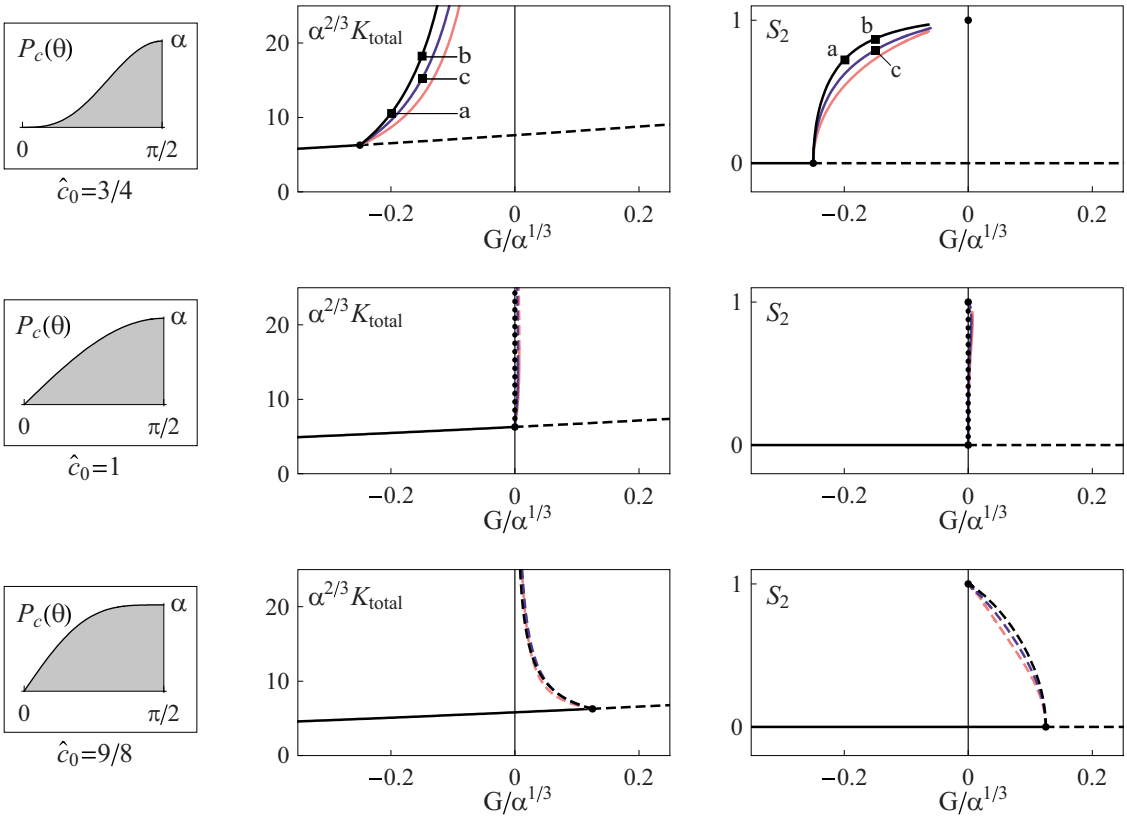

FIG. 4. (Color online) Bifurcation diagrams for the simplified interaction functions using three different induced catastrophe parameters. The figures on the left depict the probability $P_c(\theta)$ to induce a catastrophe upon collision, along with the corresponding values of $\hat{c}_0$. The center and right columns depict the corresponding bifurcation diagrams as a function of G, expressed in terms of the total density K_{total} and the 2D nematic order parameter S_2, respectively, where $K_{\text{total}}=\int K(\theta)d\theta$. The isotropic solutions are by definition disordered, so $S_2=0$, and their density is computed from Eq. (42). The bifurcation point is determined using Eq. (50), with $\hat{c}_2=-1/2$. For each diagram, ordered solutions have been computed for $\hat{z}_0=0$ (black), $\hat{z}_0=1$ (blue/dark gray) and $\hat{z}_0=10$ (red/light gray). The solutions have been computed using the method discussed in appendix A. Solid lines indicate stable solutions and dashed lines indicate unstable solutions (see also Sec. III E). Note that the case of $\hat{c}_0=1$ in the absence of zippering is a singular case where the stability cannot be determined, because non-isotropic solutions only exist for $G=0$. This has been indicated by a dotted line. The S_2-diagrams include the asymptotic limit point at $G=0$ with absolute ordering (at infinite density). The labels *a*, *b* and *c* indicate the parameter values of the results depicted in Fig. 5. The fact that the solutions for S_2 in the case $\hat{c}_0=\frac{3}{4}$ do not reach the asymptotic point ($G=0$, $S_2=1$) is a consequence of the slowdown in convergence of the path-following method as $G\uparrow 0$.

It should be noted that the absolute value of the prefactor α has no qualitative effect on the results. This can be understood by realizing that the set of Eqs. (35e) is invariant under the scaling

$$\mathbf{C}\to\gamma\mathbf{C} \quad L\to\gamma^{-1/3}L$$

$$\mathbf{Z}\to\gamma\mathbf{Z} \quad K\to\gamma^{-2/3}K$$

$$G\to\gamma^{1/3}G \quad T\to\gamma^{-1/3}T,$$

where $\gamma>0$ is an arbitrary positive scaling factor. Choosing $\gamma=\alpha^{-1}$ clearly scales away the prefactor in the definitions Eq. (56). Explicitly, the relevant parameters become $\mathbf{C}/\alpha$, $\mathbf{Z}/\alpha$, and $\alpha^{-1/3}$G and the variables $\alpha^{1/3}L$, $\alpha^{2/3}K$, and $\alpha^{1/3}T$. With this in mind, we have used the convenient choice $\alpha=1$ for our numerical calculations, indicating the appropriate scaling on the axes of Figs. 4 and 5.

Equation (50) indicates that, for the simplified interaction functions, the bifurcation point is located in the range

$$-\frac{1}{4}\le G^*\le\frac{1}{8} \tag{58}$$

and from Eqs. (42) and (54) we find that $K^*=\alpha^{-2/3}$ and $\Lambda^*=4/(\alpha\pi)$. We have used the numerical procedure described in Appendix to determine the ordered solutions of (36), starting from the bifurcation point. This has been done for nine different parameter values. For the values of $\hat{c}_0$ we used the extreme values 3/4 and 9/8, as well as 1, the latter corresponding to $G^*=0$. For each of these three cases, we have varied the zippering parameter $\hat{z}_0$, choosing values of 0, 1, and 10. Figure 4 shows the results, depicting both the total density of the system and the degree of ordering as a function of G. The degree of ordering is measured by the order parameter S_2, defined as

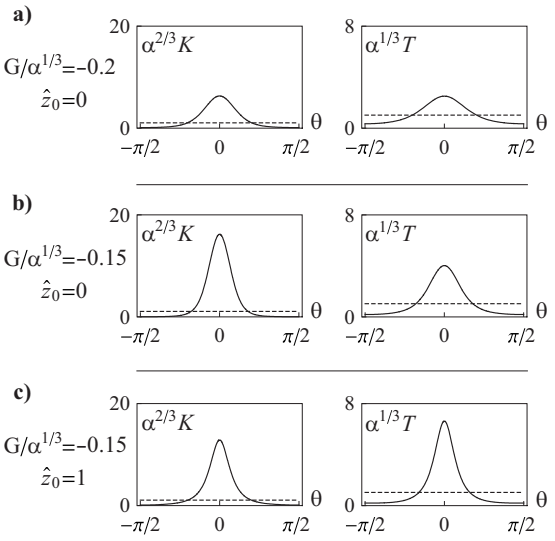

FIG. 5. Three stable ordered solutions that correspond to the points labeled (a), (b), and (c) in Fig. 4. The (unstable) isotropic solutions for the same parameter values are indicated with a dashed line. The parameter values for (a) and (b) differ only in the value of G, whereas the parameter values for (b) and (c) differ only in the value of $\hat{z}_0$. All results have been calculated using the method described in appendix A.

$$S_2 = \frac{\left| \int_0^{2\pi} d\theta e^{i2\theta} K(\theta) \right|}{\int_0^{2\pi} d\theta K(\theta)}. \tag{59}$$

This order parameter yields a value of 0 for a completely disordered system and a value of 1 for a fully oriented system, and is commonly used to describe the apolar order in 2D nematic liquid crystals.

E. Stability of solutions

The bifurcation constraint Eq. (47) indicates that the space of bifurcating functions κ_n is spanned by the functions $\cos(2n\theta)$ and $\sin(2n\theta)$ for a given value of $n \geq 1$. These solutions are therefore symmetric with respect to an arbitrary axis that we choose to place at $\theta=0$. Even after the restriction to this symmetry axis there are still two solution branches emanating from the bifurcation point, differing in the sign of the coefficient of the perturbation. These branches correspond to solutions peaked around $\theta=0$ and $\theta=\pi/(2n)$, respectively, that are identical except for this rotation. The symmetry of these solutions indicates that the bifurcation is of the pitchfork type. In Fig. 5 we plot the solutions with a maximum at $\theta=0$.

The presence of a pitchfork bifurcation implies a loss of stability of the originating branch [29]. In our system, we know that the isotropic solution must be stable in the limit $G \to -\infty$. Therefore, the local stability of the isotropic solution is lost at the first bifurcation point (for the lowest value of G), corresponding to the eigenfunction $\cos(2\theta)$. Because this eigenfunction is orthogonal to the eigenfunctions related to the subsequent bifurcation points $[\cos(n\theta), n>2]$, the stability of the unstable mode will not be regained at any point along the isotropic solution and the isotropic solution itself remains unstable for all higher values of G. This also means that the solution branches originating at further pitchfork bifurcations will be unstable near the isotropic solution. In this paper, we restrict ourselves to the analysis of the first bifurcation point and the corresponding ordered solution branch. Because the solutions on this branch already have the lowest symmetry permitted by the interaction functions, there are no further bifurcation points along this branch.

Generically ([29], chap. IV), the branches of the initial pitchfork bifurcation are stable for a supercritical bifurcation (branches bending toward higher values of G) and unstable for a subcritical bifurcation (branches bending toward lower values of G). In addition, turning points in the bifurcating branches generally correspond to an exchange of stability ([30], p. 22). This analysis allows us to assign stability indicators to the bifurcation diagrams in Fig. 4, even in the absence of a detailed study of the time-dependent Eqs. (1).

IV. DISCUSSION AND CONCLUSIONS

Based on biological observations, we have constructed a model for the orientational alignment of cortical microtubules. The model has a number of salient features. First of all, for a given set of induced catastrophe and zippering probabilities $[P_c(\theta)$ and $P_z(\theta)]$, it allows us to identify a single dimensionless control parameter G, which is fully determined by the nucleation rate and intrinsic dynamics of individual microtubules. This result by itself may turn out to be very useful in comparing different *in vivo* systems or the same system under different conditions or in different developmental stages. For increasing values of G, the isotropic stationary solutions to the model show an increase both in density and in abundance of interactions, as measured by the ratio of microtubule length to the mesh-size.

Second, the bifurcation point, i.e., the critical value of G^* of the control parameter at which the system develops ordered stationary solutions from the isotropic state, is determined solely by the probability of collisions between microtubules that lead to an induced catastrophe. Moreover, the numerical solutions of the minimal model introduced in Sec. III D show that the system can exhibit ordered stationary states when only catastrophe inducing collisions are taken into account. Perhaps surprisingly the results with zippering collisions switched on show that the co-alignment of microtubules due to the zippering events, if anything, diminishes the degree of order (at least for the values of the relative strength of zippering considered). These results strongly suggest that the "weeding out" of misaligned microtubules—by marking them for early removal by the induced switch to the shrinking state—is the driving force for the ordering process.

While due to the inherent complexity of the model it is not easy to get an intuitive understanding of the different effects of zippering and induced catastrophes, one feature that clearly distinguishes them is their different effect on microtubule lifetimes. The occurrence of an induced catastrophe will shorten the lifetime of the current segment,

thereby actively repressing segments in a minority direction. Zippering, on the other hand, reorients the growing tip, but leaves the expected lifetime of the newly inactivated segment intact. As a result, any discordant tails of microtubules will have a longevity equal to that of the segments in a potentially dominant orientation.

Furthermore, in spite of not being able to directly assess the stability of the solutions in the time domain, we have provided arguments that stable ordered solutions are possible only for the regime $G<0$, i.e., where the length of individual microtubules is intrinsically bounded. For $G>0$, individual microtubules have the tendency to grow unbounded, unless they are kept in check by catastrophic collisions. Although (locally) stable solutions may exist for values of G that are not too large, for every $G>0$ there exists a class of aligned 'runaway' solutions with diverging densities. The computed ordered solutions, regardless of their stability, converge to a point with $G=0$, for which the microtubules are perfectly aligned ($S_2=1$) and the system is infinitely dense. The existence of this point can be understood by the fact that the alignment also serves to decrease the number of collisions, and in the limit of a perfectly aligned system, the (relative) number of collisions vanishes.

How realistic is the model presented? To address this question we first discuss the effect of our use of homogeneous densities to describe the microtubule segments. Effectively, the microtubules have no determined position, and therefore, as in any mean fieldlike approach, spatial correlations between microtubules are ignored. This arguably leads to inaccuracies in the dynamical behavior of microtubules. For example, consider what happens when a microtubule starts shrinking as a result of a collision with another microtubule. In a real system, where the microtubule has a definite position, if the microtubule returns to the growing state following a rescue event, it is likely to collide with the same microtubule as before. In our homogeneous approximation, such correlations are ignored. To investigate the resulting error, the theory presented here should be compared with the results from explicit particle-based simulations. Initial results that we have presented in [31] suggest that these correlations (in the absence of zippering) do not have a significant effect.

When zippering is enabled, the problem of ignoring the spatial correlations described above extends to situations where a microtubule is shrinking away from another microtubule after undoing a zippering event. However, the homogeneity assumption also gives rise to a second and arguably more important effect: the inability to properly account for microtubule bundles. Whenever a microtubule zippers alongside another segment, they form a parallel bundle [32]. The coarse-grained nature of our model precludes the formation of bundles and only allows for alignment of the segments. This means that a microtubule that is growing in a different direction encounters each microtubule separately rather than as a single bundle. It is to be expected that the catastrophe and zippering rates stemming from N individual collisions will be higher than those from a single collision with a bundle of N microtubules. For this reason the event rate in realistic systems is likely to be lower than that predicted by the model. Furthermore, real microtubule bundles are thought to be more than simply adjacently aligned microtubules, because they may be stabilized through association with bundling proteins that could potentially decrease the catastrophe rate of individual microtubules within a bundle (see [33]). We have begun to investigate the effect of bundling in simulations with different bundle-dependent collision dynamics, presented in [31]. Using two extreme models of bundle collision dynamics we observed significant contributions of zippering but these varied in sign and remained smaller than the dominant influence of catastrophic collisions. To further quantify the effect of zippering, the model presented here would need to be extended to address bundling and (an approximation of) the correlations mentioned above.

We also need to consider several known biological factors that have not been included in the present model. The first of these is that microtubules typically can deattach from their nucleation sites and then perform so called treadmilling motion, whereby the minus-end shrinks at a more or less steady pace, which is small compared to both the growth and the shrinking speed of the more active plus end. In the case that no zippering occurs at all it is relatively easy to show that the effect of treadmilling simply leads to a renormalization of the parameter G and the interaction functions $c(\theta)$ and $z(\theta)$, but leaves the qualitative behavior of the model identical to the one discussed here. When zippering does occur, one expects the treadmilling to enhance the degree of ordering in an ordered state, as over time it "eats-up" the, by definition less ordered, initial segments of each microtubule. This effect is also consistent with the observation in Fig. 5(c) that in the case with zippering the active tips are on average more strongly aligned than the average segment. In fact, given that the comparison between Figs. 5(b) and 5(c) also shows that, all else being equal, zippering sharpens the orientational distribution of the active tips as compared to the case with no zippering, it is conceivable that the combination of zippering and treadmilling could lead to more strongly ordered systems for the same value of the control parameter.

Next it is known that *in vivo* severing proteins, such as katanin are active in, and crucial to, the formation of the cortical array [34]. Although in principle the effect of severing proteins could be included in the model, it would present formidable problems in the analysis as well as introduce additional parameters into the model for which precise data is lacking.

Finally, our model implicitly assumes that there is an infinite supply of free tubulin dimers available for incorporation into microtubules. Although there is no definite experimental evidence for this, it is reasonable to assume that *in vivo* there is a limit to the size of the free tubulin pool. Such a finite tubulin pool would have marked consequences for the behavior of the model, because the growth speed, and possibly also the nucleation rate, are dependent on the amount of free tubulin, or equivalently the total length density of microtubules k_{tot}. To a first approximation the growth speed is given by $v^+(k_{tot})=v^+(k_{tot}=0)(1-\frac{k_{tot}}{k_{\max}})$ where $k_{\max}$ the maximally attainable length density when all tubulin is incorporated into microtubules [35]. This allows for stable states to develop even when $G(k_{tot}=0)>0$, because under this pool-size constraint the length of individual microtu-

bules will always remain bounded, and the system will settle into a steady state with $G(k_{tot}) < G(k_{tot}=0)$. This behavior could provide a biologically motivated mechanism by which a solution with a particular density is selected.

To see whether our model, in spite of its approximate nature, makes sense in the light of the available data we first use the collision event probabilities obtained by Dixit and Cyr [15] (see Fig. 3) to obtain an estimate for the bifurcation value of the control parameter of $G^*=-0.15$ for the case of Tobacco BY-2 cells. An ordered phase of cortical microtubules should therefore be possible provided $G>G^*$. Given the available data on the microtubule instability parameters in this same system taken from Dhonukshe *et al.* [10] and Vos *et al.* [36] we would predict using the definition (36e) that this requires the nucleation rate of new microtubules to be larger than 0.05 min^{-1} μm^{-2} (Dhonukshe) and 0.01 min^{-1} μm^{-2} (Vos), respectively. Both these estimates for a lower bound on the nucleation rate are reasonable as they imply the nucleation of order 10^3 microtubules in the whole cortex over the course of the build-up toward full transverse order, comparable to the number that is observed.

Finally, we should point out that our model so far only addresses the question of what causes cortical microtubules to align with respect to each other. Given that in growing plant cells the cortical array is invariably oriented transverse to the growth direction, the question of what determines the direction of the alignment axis with respect to the cell axes is as, if not more, important from a biological perspective. We hope to address this question, as well as the influence of some of the as yet neglected factors mentioned above, in future work.

ACKNOWLEDGMENTS

The authors thank Kostya Shundyak, Jan Vos, and Jelmer Lindeboom for helpful discussions. S.H.T. is grateful to Jonathan Sherratt for his comments on the stability of solutions. R.J.H. was supported by a grant within the EU Network of Excellence "Active Biomics" (Contract No. NMP4-CT-2004-516989). S.H.T. was supported by a grant from the NWO program "Computational Life Sciences" (Contract No. CLS 635.100.003). This work is part of the research program of the "Stichting voor Fundamenteel Onderzoek der Materie (FOM)," which is financially supported by the "Nederlandse organisatie voor Wetenschappelijk Onderzoek (NWO)."

APPENDIX: NUMERICAL EVALUATION OF THE ORDERED SOLUTIONS

The solutions to the set of Eqs. (36) lie in an infinite-dimensional solution space. This creates significant hurdles for the numerical search for solutions. In this section, we will see that it is possible to restrict the solutions to a finite-dimensional space by imposing constraints on the interaction operators **C** and **Z**. In addition, we present a method to follow the branch of ordered solution in this finite-dimensional space, starting from the bifurcation point Eq. (50).

We start by reformulating the set of Eqs. (36) by replacing $L(\theta)$ and $T(\theta)$ through the definitions

$$S(\theta) = \frac{1}{L(\theta)}, \quad U(\theta) = \frac{1}{K(\theta)}\left[\frac{T(\theta)}{L(\theta)} - 1\right]. \tag{A1}$$

Following these substitutions, the interaction operators are all applied at the outermost level of the equations, enabling us to make use of their properties in Fourier space. Explicitly, we obtain

$$S(\theta) = -G + \mathbf{C}[K](\theta) + \mathbf{Z}[K](\theta) \tag{A2}$$

$$Q(\theta) = \mathbf{Z}[K(1+Q)/S](\theta) \tag{A3}$$

$$U(\theta) = \mathbf{Z}[(1+KU)/S](\theta) \tag{A4}$$

and

$$K(\theta) = \frac{1+Q(\theta)}{S^2(\theta) - U(\theta)[1+Q(\theta)]}. \tag{A5}$$

Denoting the Fourier components of $S(\theta)$, $Q(\theta)$ and $U(\theta)$, by $\hat{s}_n$, $\hat{q}_n$ and $\hat{u}_n$, respectively, the interacting microtubule equations reduce to a (potentially infinite) set of scalar integral equations:

$$\hat{s}_{2n} = -2\delta_{n,0}G + \frac{\hat{c}_{2n}+\hat{z}_{2n}}{\pi}\int_0^{2\pi} d\theta \cos(2n\theta)K(\theta) \tag{A6a}$$

$$\hat{q}_{2n} = \frac{\hat{z}_{2n}}{\pi}\int_0^{2\pi} d\theta \frac{\cos(2n\theta)K(\theta)[1+Q(\theta)]}{S(\theta)} \tag{A6b}$$

$$\hat{u}_{2n} = \frac{\hat{z}_{2n}}{\pi}\int_0^{2\pi} d\theta \frac{\cos(2n\theta)[1+K(\theta)U(\theta)]}{S(\theta)}. \tag{A6c}$$

From the structure of these equations, we immediately see that we can greatly reduce the dimensionality of the problem by setting a number of Fourier coefficients $\hat{z}_{2n}$ and $\hat{c}_{2n}$ to zero. In other words, by restricting our space of interaction functions $c(\theta)$ and $z(\theta)$, the problem can be reduced to a finite number of scalar equations.

Applied to the simplified interaction functions introduced in Sec. III D, we know that the sets of stationary solutions form lines in the eight-dimensional phase space spanned by the variables $\{\hat{s}_0, \hat{s}_2, \hat{s}_4, \hat{q}_0, \hat{q}_4, \hat{u}_0, \hat{u}_4\}$ and the parameter G. At least two such solution lines exist, one corresponding to the isotropic solution and the other to the ordered solution, and these lines intersect at the bifurcation point.

Within this 8-dimensional space, we have used a numerical path-following method similar to the one described in [37,38] that follows the ordered solution branch by searching for a local minimum in the root mean error of the constituent Eqs. (A5). The search for ordered solutions is initiated at the bifurcation point, with coordinates

$$S^* = \frac{\hat{z}_0 - 2\hat{c}_2}{(-2\hat{c}_2)^{2/3}}, \quad Q^* = -\frac{\hat{z}_0}{2\hat{c}_2}, \quad U^* = \frac{\hat{z}_0}{(-2\hat{c}_2)^{1/3}}, \tag{A7}$$

so that in the case of our simplified interaction model

$$\{G,\hat{s}_0,\hat{s}_2,\hat{s}_4,\hat{q}_0,\hat{q}_4,\hat{u}_0,\hat{u}_4\}_0 = \{c_0-1,2(\hat{z}_0+1),0,0,2\hat{z}_0,0,2\hat{z}_0,0\}. \quad \text{(A8)}$$

The initial instability affects only the $\cos(2\theta)$ mode. This mode only appears in the equation for $\hat{s}_2$ and the remaining parameters are affected only by higher order corrections. For this reason we choose the initial direction of the path to be the unit vector in the $\hat{s}_2$ direction and the path is traced from there.

[1] Bruce Alberts, Alexander Johnson, Julian Lewis, Martin Raff, Keith Roberts, and Peter Walter. *Molecular Biology of the Cell*, 4th ed. (Garland Science, New York, 2002).
[2] D. W. Ehrhardt and S. L. Shaw, Annu. Rev. Plant Biol. **57**, 859 (2006).
[3] A. Paradez, A. Wright, and D. W. Ehrhardt, Curr. Opin. Plant Biol. **9**, 571 (2006).
[4] D. J. Cosgrove, Nat. Rev. Mol. Cell Biol. **6**, 850 (2005).
[5] G. O. Wasteneys and R. E. Williamson, Eur. J. Cell Biol. **50**, 76 (1989).
[6] F. Kumagai, A. Yoneda, T. Tomida, T. Sano, T. Nagata, and S. Hasezawa, Plant Cell Physiol. **42**, 723 (2001).
[7] S. L. Shaw, R. Kamyar, and D. W. Ehrhardt, Science **300**, 1715 (2003).
[8] J. W. Vos, B. Sieberer, A. C. J. Timmers, and A. M. C. Emons, Cell Biol. Int. **27**, 295 (2003).
[9] A. R. Hardham and B. E. Gunning, J. Cell Biol. **77**, 14 (1978).
[10] P. Dhonukshe, A. M. Laxalt, J. Goedhart, T. W. J. Gadella, and T. Munnik, Plant Cell **15**, 2666 (2003).
[11] J. C. Gardiner, J. D. Harper, N. D. Weerakoon, D. A. Collings, S. Ritchie, S. Gilroy, R. J. Cyr, and J. Marc, Plant Cell **13**, 2143 (2001).
[12] T. Hashimoto and T. Kato, Curr. Opin. Plant Biol. **9**, 5 (2006).
[13] T. Hamada, J. Plant Res. **120**, 79 (2007).
[14] V. Kirik, U. Herrmann, C. Parupalli, J. C. Sedbrook, D. W. Ehrhardt, and M. Hülskamp, J. Cell. Sci. **120**, 4416 (2007).
[15] R. Dixit and R. Cyr, Plant Cell **16**, 3274 (2004).
[16] A. Mogilner, E. Geigant, and K. Ladizhansky, SIAM J. Appl. Math. **59**, 787 (1998).
[17] K. Kruse, J. F. Joanny, F. Jülicher, J. Prost, and K. Sekimoto, Eur. Phys. J. E **16**, 5 (2005).
[18] I. S. Aranson and L. S. Tsimring, Phys. Rev. E **74**, 031915 (2006).
[19] V. Rühle, F. Ziebert, R. Peter, and W. Zimmermann, Eur. Phys. J. E **27**, 243 (2008).
[20] S. Portet, J. A. Tuszynski, J. M. Dixon, and M. V. Sataric, Phys. Rev. E **68**, 021903 (2003).
[21] K. Doubrovinski and K. Kruse, Phys. Rev. Lett. **99**, 228104 (2007).
[22] A. Zumdieck, M. Cosentino Lagomarsino, C. Tanase, K. Kruse, B. M. Mulder, M. Dogterom, and F. Jülicher, Phys. Rev. Lett. **95**, 258103 (2005).
[23] V. A. Baulin, C. M. Marques, and F. Thalmann, Biophys. Chem. **128**, 231 (2007).
[24] M. Dogterom and S. Leibler, Phys. Rev. Lett. **70**, 1347 (1993).
[25] T. Murata, S. Sonobe, T. I. Baskin, S. Hyodo, S. Hasezawa, T. Nagata, T. Horio, and M. Hasebe, Nat. Cell Biol. **7**, 961 (2005).
[26] T. Murata and M. Hasebe, J. Plant Res. **120**, 73 (2007).
[27] R. L. Margolis and L. Wilson, BioEssays **20**, 830 (1998).
[28] M. E. Janson, M. E. de Dood, and M. Dogterom, J. Cell Biol. **161**, 1029 (2003).
[29] M. Golubitsky and D. G. Schaeffer, *Singularities and Groups in Bifurcation Theory* (Springer-Verlag, Berlin, 1984), Vol. 1.
[30] G. Iooss and D. D. Joseph, *Elementary Stability and Bifurcation Theory* (Springer-Verlag, Berlin, 1980).
[31] S. H. Tindemans, R. J. Hawkins, and B. M. Mulder, Phys. Rev. Lett. **104**, 058103 (2010).
[32] D. A. Barton, M. Vantard, and R. L. Overall, Plant Cell **20**, 982 (2008).
[33] J. Gaillard, E. Neumann, D. van Damme, V. Stoppin-Mellet, C. Ebel, E. Barbier, D. Geelen, and M. Vantard, Mol. Biol. Cell **19**, 4534 (2008).
[34] A. Roll-Mecak and R. D. Vale, J. Cell Biol. **175**, 849 (2006).
[35] T. Mitchison and M. Kirschner, Nature (London) **312**, 237 (1984).
[36] J. W. Vos, M. Dogterom, and A. M. C. Emons, Cell Motil. Cytoskeleton **57**, 246 (2004).
[37] E. L. Allgower and K. Georg, *Introduction to Numerical Continuation Methods*, Classics in Applied Mathematics (SIAM, Philadelphia, 2003), Vol. 45.
[38] P. Deuflhard, B. Fiedler, and P. Kunkel, SIAM (Soc. Ind. Appl. Math.) J. Numer. Anal. **24**, 912 (1987).